

# Role of non-magnetic spacers in the magnetic interactions of antiferromagnetic topological insulators $\text{MnBi}_4\text{Te}_7$ and $\text{MnBi}_2\text{Te}_4$

Bing Li,<sup>1,2,\*</sup> D. M. Pajerowski,<sup>3</sup> J.-Q. Yan,<sup>3</sup> and R. J. McQueeney<sup>1,2</sup>

<sup>1</sup>Ames National Laboratory, Ames, IA, 50011, USA

<sup>2</sup>Department of Physics and Astronomy, Iowa State University, Ames, IA, 50011, USA

<sup>3</sup>Oak Ridge National Laboratory, Oak Ridge, TN, 37831, USA

(Dated: February 19, 2025)

$\text{MnBi}_4\text{Te}_7$  belongs to a family of antiferromagnetic topological insulators. It forms a natural heterostructure of magnetic (septuple) and non-magnetic (quintuple) topological blocks. Here, we explore the magnetism and magnetic interactions in this compound using inelastic neutron scattering. We find that the interlayer magnetic coupling is much weaker in  $\text{MnBi}_4\text{Te}_7$  as compared to  $\text{MnBi}_2\text{Te}_4$  due to the insertion of non-magnetic quintuple layers in the former. However, other key magnetic energy scales residing within a single septuple block, the single-ion anisotropy and long-range intralayer exchanges, are essentially the same. This identifies a transferable set of magnetic interactions applicable to the extended family of magnetic topological insulators based on  $\text{MnBi}_2\text{Te}_4$ - $\text{Bi}_2\text{Te}_3$  heterostructures.

## I. INTRODUCTION

The  $\text{MnBi}_2\text{Te}_4$  (MBT) compound is the first known intrinsic antiferromagnetic topological insulator [1–3] and has been utilized as a platform to interrogate the novel phenomena in topological phases such as axion and Chern insulators [4–8]. The key to accessing these topological properties is the van der Waals (vdW) coupling between structural blocks, resulting in weak interlayer antiferromagnetic interactions. Combined with an uniaxial magnetic anisotropy of the Mn sublattice, MBT provides easily accessible metamagnetic spin-flop and forced ferromagnetic phases that host unique topological phenomena [9].

Much less explored are the extended family of  $\text{MnBi}_{2+2n}\text{Te}_{4+3n}$  compounds where MBT septuple blocks are separated by  $n$  non-magnetic  $\text{Bi}_2\text{Te}_3$  quintuple topological insulator (TI) blocks [10–15]. A single septuple block is ferromagnetic (FM), while the interlayer magnetic coupling is antiferromagnetic (AF), at least for  $n = 0, 1$ , and 2. The insertion of non-magnetic spacer blocks increases the Mn sublattice interlayer distance and, therefore, is expected to reduce the interlayer magnetic coupling, affecting the landscape of magnetic phases and magnetization dynamics [9, 14, 16–20]. The MBT family provides a means for controlled studies of the magnetization dynamics where interlayer couplings can be tuned from weak (for  $\text{MnBi}_2\text{Te}_4$ ) to essentially zero (for  $\text{MnBi}_8\text{Te}_{13}$ ) [16]. In the latter  $n = 3$  system, long-range dipolar interactions dominate the interlayer coupling, resulting in fragile ferromagnetism [21].

It has been suggested that large  $n$  MBT compounds form a new class of magnets, called single-layer magnets [16], which consist of a periodic array of magnetic layers with vanishing interlayer coupling. Thus, in addition to

the interesting topological properties, the MBT family also allows for the exploration of the interplay between dimensionality and magnetism in these unique van der Waals bonded natural heterostructures.

In the quest to understand the evolution towards single-layer magnets, here we describe inelastic neutron scattering (INS) measurements on the  $n = 1$  compound  $\text{MnBi}_4\text{Te}_7$ , and compare these results to previous measurements on the  $n = 0$  compound  $\text{MnBi}_2\text{Te}_4$  [22, 23]. In those measurements, we found  $\text{MnBi}_2\text{Te}_4$  to possess long-range and competing intralayer magnetic interactions, giving rise to a linear sawtooth-like spin wave dispersion. The uniaxial single-ion anisotropy align the Mn spins along the crystallographic  $c$ -axis, and the relatively strong AF interlayer coupling across the vdW gap ( $J_c$ ) results in the AF stacking of FM layers. The metamagnetic spin-flop transition in a magnetic field applied perpendicular to the layers can be described by a microscopic model using an Hamiltonian with exchange interactions and a single-ion anisotropy, using parameters determined from INS measurements [24]. The Néel temperature for  $\text{MnBi}_2\text{Te}_4$ ,  $T_N = 24$  K, is close to  $T_N^{\text{MF}} = -\frac{S(S+1)}{3k_B} \sum_i J_i \approx 19$  K estimated from the mean-field theory, where the dominant energy scale is the FM nearest intralayer interaction  $J_1$ .

Despite having the same A-type AF magnetic ground state, however, in  $\text{MnBi}_4\text{Te}_7$  the spin-flop transition is absent [9]. Together with a reduction of  $T_N = 14$  K, these suggest modifications of the magnetic interactions due to the presence of the non-magnetic spacers. In our neutron experiments described here, we find that  $\text{MnBi}_4\text{Te}_7$  has a strongly suppressed interlayer spin wave bandwidth and a reduction in the spin gap compared to  $\text{MnBi}_2\text{Te}_4$ . Both observations are consistent with vanishing interlayer exchange coupling and a transferable single-ion anisotropy. Without the influence from the interlayer couplings, the interactions within a single septuple block could be more reliably determined using the linear spin wave theory (LSWT) analysis based

\* Current address: Neutron Scattering Division, Oak Ridge National Laboratory, Oak Ridge, TN, 37831, USA

on the Heisenberg model. This analysis confirms that long-range and competing intralayer interactions found in  $\text{MnBi}_2\text{Te}_4$  are intrinsic to the septuple blocks in all MBT family members.

Overall, this suggests that  $\text{MnBi}_4\text{Te}_7$  and successive  $n > 1$  MBT family members are quite close to the 2D limit. Considering that INS is a bulk measurement, we propose that  $\text{MnBi}_4\text{Te}_7$  serves as a suitable system to probe 2D magnetism, which is not only interesting theoretically but also relevant for the development of few-layer magnetic TI devices [19, 25–27].

## II. EXPERIMENTAL DETAILS

Single-crystal samples of  $\text{MnBi}_4\text{Te}_7$  and  $\text{MnBi}_2\text{Te}_4$  were grown out of a Bi-Te flux [12]. The elemental analysis and X-ray and neutron diffraction results reveal that the Mn site hosts extra Bi and Mn vacancies, giving a chemical formula of  $\text{Mn}_{0.8}\text{Bi}_{4.2}\text{Te}_7$ .  $\text{MnBi}_2\text{Te}_4$  crystallizes in space group  $R\bar{3}m$  (#166), with lattice parameters  $a = b = 4.33 \text{ \AA}$ ,  $c = 40.91 \text{ \AA}$  whereas  $\text{MnBi}_4\text{Te}_7$  crystallizes in space group  $P\bar{3}m1$  (#164), with lattice parameters  $a = b = 4.366 \text{ \AA}$ ,  $c = 23.80 \text{ \AA}$ . The essential difference between the two chemical structures is the close-packed stacking of magnetic Mn sublattice in the former and the simple hexagonal stacking in the latter. A comparison of the two crystal structures is shown in Fig. 1(a) and (b).

For both compounds, the 2D projection of the Brillouin zone is hexagonal and we define reciprocal space vectors  $\mathbf{q} = \frac{4\pi}{\sqrt{3}a}(H\hat{a}^* + K\hat{b}^*) + \frac{2\pi}{c}L\hat{c}^*$  and special points  $\Gamma = (0, 0, 0)$ ,  $M = (1/2, 0, 0)$ ,  $K = (1/3, 1/3, 0)$ . SQUID measurements for  $\text{MnBi}_4\text{Te}_7$  confirm that AFM ordering occurs at  $T_N = 13.7 \text{ K}$  and neutron diffraction finds a magnetic propagation vector of  $\boldsymbol{\tau} = (0, 0, \frac{1}{2})$ , consistent with the A-type AFM order [12]. Previous reports of  $\text{MnBi}_2\text{Te}_4$  find  $T_N = 24.7 \text{ K}$  and  $\boldsymbol{\tau} = (0, 0, \frac{3}{2})$  for the A-type order of Mn layers with rhombohedral stacking [3].

Similar to  $\text{MnBi}_2\text{Te}_4$ , the INS measurements on  $\text{MnBi}_4\text{Te}_7$  were performed using the Cold Neutron Chopper Spectrometer (CNCS) at the Spallation Neutron Source in Oak Ridge National Laboratory. Co-aligned single-crystal samples with a total mass of 503.7 mg [28] were mounted to a top-loading orange cryostat. Measurements were performed using the incident energies  $E_i = 3.32$  and  $1.55 \text{ meV}$  at base temperatures  $T = 2 \text{ K}$ . Measurements at higher temperatures were also taken for the estimation of background signals.

## III. RESULTS

Spin waves along high-symmetry directions in  $\text{MnBi}_4\text{Te}_7$  are shown in Fig. 1(c-e), compared to spin waves in  $\text{MnBi}_2\text{Te}_4$  shown in Fig. 1(f-h) which are originally reported in Ref. [22]. The intensity is multiplied by energy transfer  $E$  to enhance the contrast at higher

$E$ . Square brackets are used to denote the range of summation in  $\mathbf{q}$  in reciprocal lattice units. Three orthogonal axes used to denote  $\mathbf{q}$  are  $(H, H, 0)$ ,  $(-K, K, 0)$ , and  $(0, 0, L)$ . For  $\text{MnBi}_4\text{Te}_7$  in Fig. 1(c) and (d),  $L = [2, 6]$ .  $H = [-0.05, 0.05]$  in (c), and  $K = [-0.05, 0.05]$  in (d). In (e),  $H = K = [-0.04, 0.04]$ . For  $\text{MnBi}_2\text{Te}_4$  in Fig. 1(f) and (g),  $L = [0, 20]$  for  $E_i = 6.6 \text{ meV}$  data and  $L = [3, 12]$  for  $E_i = 3.3 \text{ meV}$  data.  $H = [-0.05, 0.05]$  in (f), and  $K = [-0.05, 0.05]$  in (g). In (h),  $H = K = [-0.02, 0.02]$ .

Comparison of Figs. 1(c) with 1(f) and Figs. 1(d) with 1(g) indicate that the in-plane dispersions of  $\text{MnBi}_4\text{Te}_7$  and  $\text{MnBi}_2\text{Te}_4$  are quite similar. One obvious difference is the slightly lowered spin wave energy maximum (from  $3.3 \text{ meV}$  to  $2.3 \text{ meV}$ ), and concomitantly the smaller spin gap in  $\text{MnBi}_4\text{Te}_7$ . A comparison of the interlayer dispersions along  $L$  in Figs. 1(e) with 1(h) highlights that the interlayer coupling is strongly reduced in  $\text{MnBi}_4\text{Te}_7$ .

We discuss these features of the spin wave spectrum using LSWT based on the following Heisenberg model,

$$\mathcal{H} = \sum_{\langle ij \rangle, \parallel} J_{ij} \mathbf{S}_i \cdot \mathbf{S}_j - D \sum_i (S_i^z)^2. \quad (1)$$

This model is similar to that used in the analysis of  $\text{MnBi}_2\text{Te}_4$  [22]. The difference is that we use a 2D model for  $\text{MnBi}_4\text{Te}_7$  where the interlayer coupling terms  $J_c \sum_{\langle ij \rangle, \perp} \mathbf{S}_i \cdot \mathbf{S}_j$  are not included. In the next section, we justify this choice by showing that the reduced dispersion along  $L$  is too small to resolve  $J_c$  with our current data.

### A. Interlayer couplings

In Fig. 2, the experimental data of the interlayer dispersion is compared to simulations of the data from linear spin wave theory. For  $\text{MnBi}_2\text{Te}_4$ , one finds that the AFM interlayer coupling has two effects. It creates an oscillatory dispersion along  $(0, 0, L)$  [Fig. 2(c)] as well as a variation of scattering intensities [Fig. 2(d)]. In the latter case, the intensities having maxima at  $L = 3n \pm \frac{3}{2}$  and minima at  $L = 3n$  which result from the AFM propagation vector of  $\boldsymbol{\tau} = (0, 0, 3/2)$ , corresponding to staggered magnetization of hexagonal close-packed magnetic layers.

In  $\text{MnBi}_4\text{Te}_7$ , however, neither of the two effects are clearly observed. Analysis on the spin wave dispersion along  $(0, 0, L)$  gives a single-ion anisotropy  $SD_z = 0.077(1) \text{ meV}$ , similar to the value  $SD_z = 0.0814 \text{ meV}$  in  $\text{MnBi}_2\text{Te}_4$  reported in Ref. [22], and an unstable interlayer interaction  $SJ_c = 0.001(1) \text{ meV}$  [28], in comparison to  $SJ_c^{124} = 0.065(2) \text{ meV}$  [22]. Integrated intensities at low  $E = [0.15, 0.35] \text{ meV}$  are plotted in Fig. 2(b) for  $\text{MnBi}_4\text{Te}_7$  along  $(0, 0, L)$  together with the simulated intensities with  $SJ_c = 0$  and  $SJ_c = 0.02 \text{ meV}$ . Due to the simple stacking of hexagonal magnetic layers in  $\text{MnBi}_4\text{Te}_7$ , the intensity maxima are expected at  $L = n \pm \frac{1}{2}$ . However, no distinctive intensity variations are observed with the current counting statistics. For

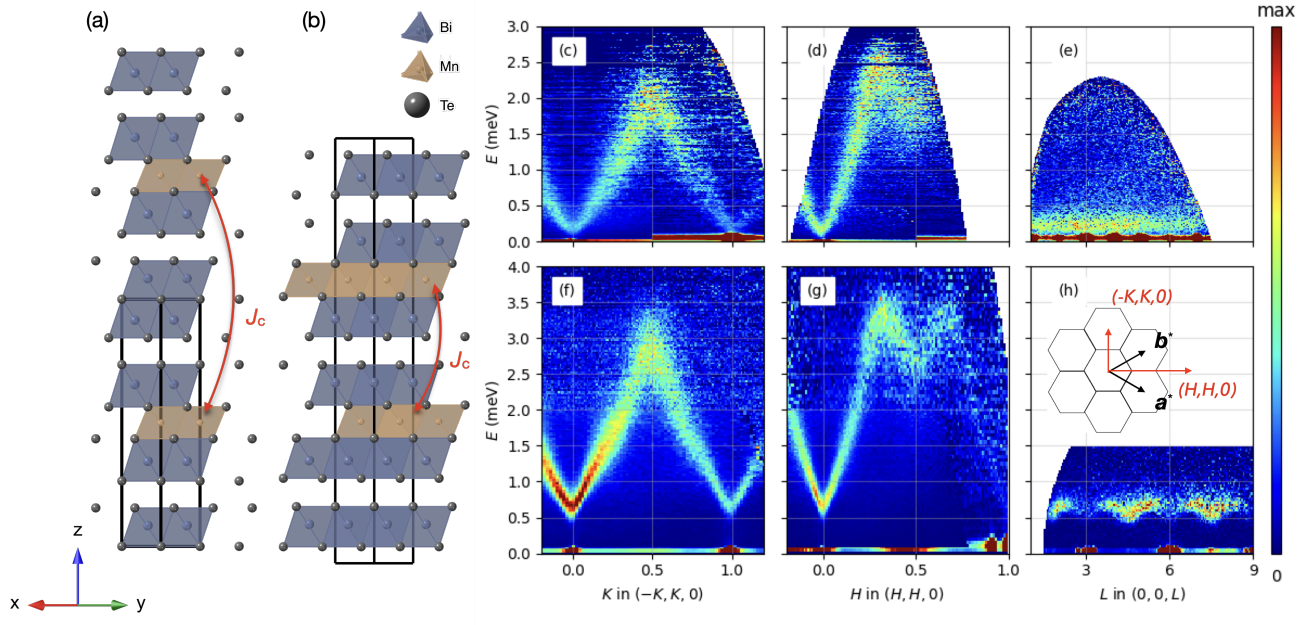


FIG. 1. Crystal structure of (a)  $\text{MnBi}_4\text{Te}_7$  and (b)  $\text{MnBi}_2\text{Te}_4$  with  $J_c$  indicating the distance of the nearest interlayer neighbor. (c-e) Spin waves in  $\text{MnBi}_4\text{Te}_7$  measured at  $T = 2$  K with  $E_i = 3.32$  meV. Measurement with  $E_i = 1.55$  meV is overlaid on top in (c) and (d) for better visualization of the spin gap at low  $E$ . (f-h) Spin waves in  $\text{MnBi}_2\text{Te}_4$  measured at  $T = 2$  K with  $E_i = 6.6$  meV, with  $E_i = 3.3$  meV measurement overlaid on top in (f) and (g). The intensity in (c-h) is multiplied by energy transfer  $E$  to enhance the contrast at higher  $E$ . Inset of (h) shows the 2D projection of the Brillouin zone and the high-symmetry directions.

example, with  $SJ_c \geq 0.02$  meV, Fig 2(b) shows that the variation of intensities should be significant enough to be observed. Therefore we estimate an upper limit of  $SJ_c = 0.02$  meV for the interlayer coupling in  $\text{MnBi}_4\text{Te}_7$ .

It is worth mentioning that the difference in magnetic layer stacking results in each Mn ion in  $\text{MnBi}_4\text{Te}_7$  having only two interlayer nearest-neighbors, whereas in  $\text{MnBi}_2\text{Te}_4$  each Mn has six. Thus, the upper limit of the energy scale of the total interlayer coupling in  $\text{MnBi}_4\text{Te}_7$  is at least an order of magnitude smaller than  $\text{MnBi}_2\text{Te}_4$ .

$$\frac{2J_c^{147}}{6J_c^{124}} = \frac{2 \times 0.02}{6 \times 0.065} \lesssim 0.10. \quad (2)$$

## B. Spin gap

To investigate the single-ion anisotropy  $D$  in  $\text{MnBi}_4\text{Te}_7$ , cuts were made as functions of energy transfer  $E$  for data sets with different incident neutron energies. Figs. 3(a) and (b) show INS intensities at the bottom of the magnon band (magnetic  $\Gamma$  point)  $\mathbf{q} = (0, 0, 2.5)$  (r.l.u.), with the summation range  $H = [-0.04, 0.04]$ ,  $K = [-0.03, 0.03]$  and  $L = [2.3, 2.7]$ . The peak at  $\Delta \approx 0.2$  meV corresponds to the spin gap. Intensities at  $\mathbf{q} = (0.3, 0, 2.5)$  with the summation range of  $H$  offset to  $[0.26, 0.34]$  are used to estimate background signals from incoherent scattering. Whereas the data with

$E_i = 3.32$  meV has a coarser resolution than data with  $E_i = 1.55$  meV (orange and red), both data sets give a consistent estimate for the spin gap energy. This can be compared to the  $\Delta \approx 0.53$  meV for  $\text{MnBi}_2\text{Te}_4$  as shown in Fig. 3(b) (brown).

However, in contrast to  $\text{MnBi}_2\text{Te}_4$ , there is no clean gap in  $\text{MnBi}_4\text{Te}_7$  below which magnetic scattering intensities are completely absent. The finite spectral weight that is observed down to  $E \approx 0$  is not only a consequence of the instrumental resolution, considering that the resolution linewidth at  $E = 0$  is about 0.04 meV when  $E_i = 1.55$  meV. Rather, the broadening is caused by the intrinsic damping of the magnons that can be closely approximated as under-damped harmonic oscillators, using the spectral function,

$$F(E) \propto \frac{E \cdot \Gamma}{(E^2 - E_0^2)^2 + (E \cdot \Gamma)^2}, \quad (3)$$

where the damping factor  $\Gamma$  satisfies  $E_0^2 \geq \Gamma^2/4$ . An accurate estimation of the spin gap and the single-ion anisotropy require 2D fitting of the INS spectra with energy-resolution and  $\mathbf{q}$ -binning effects taken into consideration as performed in section III C. At  $\mathbf{q} = (0, 0, 2.5)$ , the fitting results show that the spectral function is close to being critically damped ( $E_0 \approx \Gamma/2$ ).

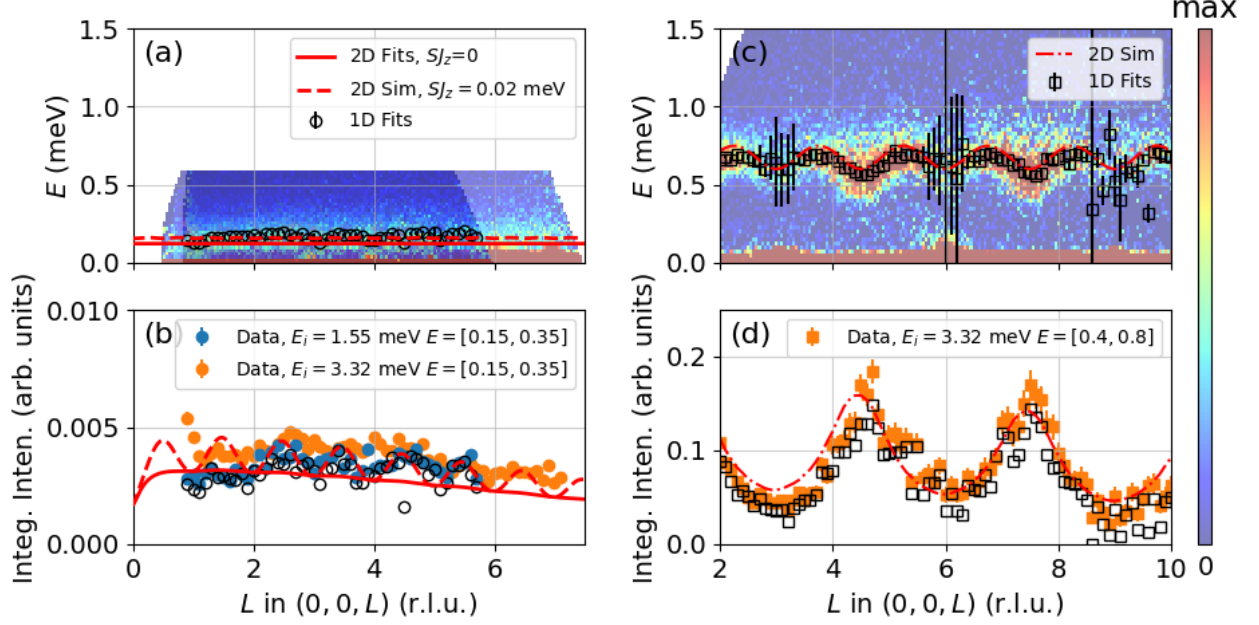


FIG. 2. Integrated INS intensities and spin wave dispersion along  $(0,0,L)$  direction for  $\text{MnBi}_4\text{Te}_7$  (a) and  $\text{MnBi}_2\text{Te}_4$  (c), similarly to data plotted in Fig. 1(e) and (f). Data with  $E_i = 1.55$  meV are overplotted on data with  $E_i = 3.32$  meV in (a). (b) and (d) show intensity variation when summed over the energy range  $E = [0.15, 0.35]$  meV and  $E = [0.4, 0.8]$  meV for  $\text{MnBi}_4\text{Te}_7$  and  $\text{MnBi}_2\text{Te}_4$ , respectively. Black open symbols with error bars are peak centers in (a) and (c), and integrated intensity in (b) and (d), obtained from fitting individual constant- $q$  line cuts. (circles for  $\text{MnBi}_4\text{Te}_7$  and squares for  $\text{MnBi}_2\text{Te}_4$ .) The large error bars in (c) result from the vanishing intensities when approaching  $L = 3n$ . Red curves show the simulated dispersion and intensity variation from fitting to the 2D slice of data. Notice that 1D and 2D fitting give consistent results in  $\text{MnBi}_2\text{Te}_4$ . Therefore, the intensity variation is used for an estimation of the upper limit of the interlayer interaction  $J_c$  in  $\text{MnBi}_4\text{Te}_7$  as shown in (b).

### C. Intralayer couplings

Given the two-dimensional nature of the spin excitations in  $\text{MnBi}_4\text{Te}_7$  with  $J_c \approx 0$ , we determine the intralayer magnetic couplings and single-ion anisotropy by using the reduced  $\chi^2$  analysis to compare the experimental and simulated spin wave intensities along  $(-K, K, 0)$  and  $(H, H, 0)$ . Starting with Eqn. (1), the analytical expression for spin wave dispersion is given by

$$\begin{aligned}
 E(\mathbf{q}) &= \sqrt{A(\mathbf{q})^2 - B(\mathbf{q})^2}, \\
 A(\mathbf{q}) &= S \left( J(\mathbf{q}) + \frac{1}{2}J(\mathbf{q} + \boldsymbol{\tau}) + \frac{1}{2}J(\mathbf{q} - \boldsymbol{\tau}) - 2J(\boldsymbol{\tau}) \right) \\
 &\quad + 2SD, \\
 B(\mathbf{q}) &= S \left( J(\mathbf{q}) - \frac{1}{2}J(\mathbf{q} + \boldsymbol{\tau}) - \frac{1}{2}J(\mathbf{q} - \boldsymbol{\tau}) \right).
 \end{aligned} \tag{4}$$

Here  $J(\mathbf{q}) = \sum_j J_{0j} e^{i\mathbf{q}\cdot\mathbf{R}_j}$  is the Fourier transformation of all neighboring magnetic interactions  $J_{ij}$  for a given atom at site  $i$ , and  $\boldsymbol{\tau} = (0, 0, \frac{1}{2})$  is the magnetic propagation vector.

The spin wave intensity  $I(\mathbf{q}, E)$  is proportional to the sum of the transverse components of the dynamic spin

correlation function  $S^{xx}(\mathbf{q}, E)$  and  $S^{yy}(\mathbf{q}, E)$ , where

$$\begin{aligned}
 S^{xx}(\mathbf{q}, E) &= S^{yy}(\mathbf{q}, E) \\
 &= S \frac{A(\mathbf{q}) - B(\mathbf{q})}{E(\mathbf{q})} \delta(E - E(\mathbf{q})) (1 - e^{-\frac{E}{k_B T}})^{-1},
 \end{aligned} \tag{5}$$

and the INS spin wave intensity  $I(\mathbf{q}, E)$  is,

$$\begin{aligned}
 I(\mathbf{q}, E) &= S |f(\mathbf{q})|^2 \frac{A(\mathbf{q}) - B(\mathbf{q})}{E(\mathbf{q})} (1 + \hat{q}_z^2) \\
 &\quad \frac{E \cdot \Gamma}{(E^2 - E_0^2)^2 + (E \cdot \Gamma)^2} (1 - e^{-\frac{E}{k_B T}})^{-1}.
 \end{aligned} \tag{6}$$

$f(\mathbf{q})$  is the magnetic form factor of  $\text{Mn}^{2+}$  ion,  $\hat{q}_z$  is the  $z$  component of the unit vector in  $\mathbf{q}$  direction and  $(1 - e^{-\frac{E}{k_B T}})^{-1}$  is the Bose thermal factor. The  $\delta$ -function in Eqn. (5) is replaced by the spectral function in Eqn. (3).

One of technical challenges for INS experiment on  $\text{MnBi}_4\text{Te}_7$  is that, since Bi and Te atoms are both heavy, the atomic percentage of Mn is much lower compared to  $\text{MnBi}_2\text{Te}_4$ . For samples with identical mass, the strength of magnetic signals in  $\text{MnBi}_4\text{Te}_7$  will be 4 times weaker than those in  $\text{MnBi}_2\text{Te}_4$ . Therefore a good estimation of the background signal is crucial for the quantitative

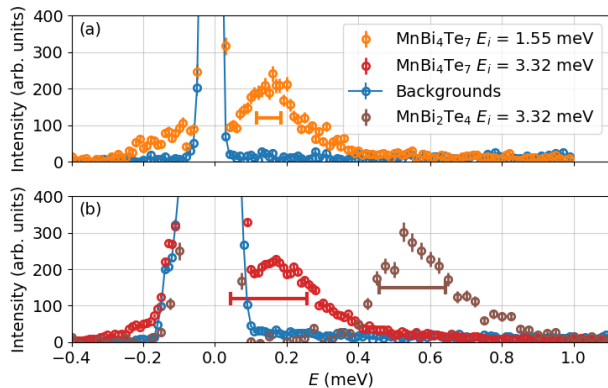


FIG. 3. Spin gap in  $\text{MnBi}_4\text{Te}_7$  at the magnetic  $\Gamma$  point, compared to  $\text{MnBi}_2\text{Te}_4$ . Orange and red circles are INS intensities at  $\mathbf{q} = (0, 0, 2.5)$ , having  $E_i = 1.55$  meV and  $3.32$  meV, respectively. Blue circles are at  $\mathbf{q} = (0.3, 0, 2.5)$ , demonstrating the incoherent background. Brown circles are INS intensities at  $\mathbf{q} = (0, 0, 4.5)$  for  $\text{MnBi}_2\text{Te}_4$ . The horizontal bars show the instrumental resolution FWHM at peak center positions.

analysis. Details of the background subtraction can be found in the supplementary information [28], including representative energy cuts of  $I(\mathbf{q}, E)$  along  $(H, H, 0)$  and  $(-K, K, 0)$ .

To account for magnon damping, cuts of  $I(\mathbf{q}, E)$  were first fit to Eqn. (6) independently to obtain the damping parameter  $\Gamma(E)$ .  $\Gamma(E)$  was then parameterized by the function  $\Gamma(E) = c_1 \arctan(c_2 E + c_3) + c_4$ . In fits to the full 2D spectra, we keep the value of the single-ion anisotropy  $SD_z = 0.077$  meV and  $J_c = 0$ , and let  $c_1, c_2, c_3, c_4$  and intralayer interactions  $J_1, \dots, J_9$  vary freely. To account for the effects of summation in  $\mathbf{q}$ , cuts of the simulations were made with the finite  $\mathbf{q}$ -binning identical to the data and compared to the data cuts. A good fit is achieved when the reduced  $\chi^2$  (sum of all  $\chi^2$  divided by the number of fitting parameters) reaches minimum where reduced  $\chi^2 = 10.82$ . The intralayer interactions are shown in Fig. 4 and the extracted strength are compiled in Table. I, together with values in  $\text{MnBi}_2\text{Te}_4$  for comparison.

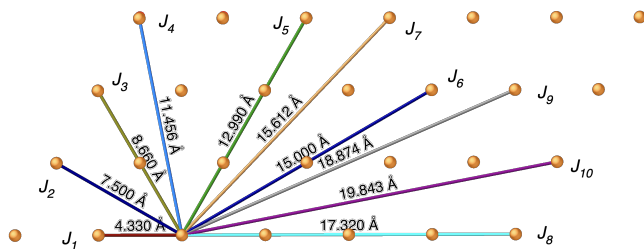


FIG. 4. Intralayer interactions and their corresponding bond lengths between Mn atoms in  $\text{MnBi}_2\text{Te}_4$  and  $\text{MnBi}_4\text{Te}_7$ .

## IV. DISCUSSION

In  $\text{MnBi}_2\text{Te}_4$ , previous reports find that the interlayer magnetic coupling  $J_c$  is relatively strong considering van der Waals nature of the magnetic coupling between  $\text{MnBi}_2\text{Te}_4$  blocks. The large spin gap ( $\Delta \approx 0.5$  meV) is consistent with the presence of the relatively strong uniaxial anisotropy. When compared to critical fields for spin-flop and saturation transitions determined from magnetization measurements, we can conclude that the uniaxial anisotropy in  $\text{MnBi}_2\text{Te}_4$  has contributions from both single-ion anisotropy and anisotropy of the interlayer exchange coupling.

In  $\text{MnBi}_4\text{Te}_7$ , we find the interlayer coupling to be negligible within the sensitivity of our measurement, consistent with the larger separation between magnetic layers. However, AF interlayer exchange coupling must still exceed the dipolar interaction that favors a global FM order. We perform a lattice sum to estimate the net FM interlayer dipolar interaction,  $J_c^{\text{dip}} = (g\mu_B)^2 \frac{\mu_0}{4\pi} \sum_j \frac{r_{0j}^2 - 3(\mathbf{r}_{0j} \cdot \hat{\mathbf{z}})^2}{r_{0j}^3}$ . By restricting the sum to include only interlayer bonds in the upper-half plane, we obtain  $J_c^{\text{dip}} \approx -0.003$  meV [28], which is smaller than the estimated upper limit of the total interlayer coupling that includes both exchange and dipolar terms ( $J_c = J_c^{\text{ex}} + J_c^{\text{dip}} \lesssim 0.01$  meV). This suggests that  $\text{MnBi}_4\text{Te}_7$  can still host AF order when interlayer AF exchange lies in an estimated range of  $0.003 \lesssim J_c^{\text{ex}} \lesssim 0.013$  meV. Ultimately, the interlayer AF exchange is exceeded by the dipolar interactions in  $\text{MnBi}_8\text{Te}_{13}$  which crosses over to FM order [21].

We now discuss the magnetic anisotropy. The local atomic configuration surrounding an Mn ion within a single septuple block is essentially the same for  $\text{MnBi}_2\text{Te}_4$  and  $\text{MnBi}_4\text{Te}_7$ . Thus, we expect that the single-ion anisotropy in the two compounds should be similar and this is confirmed by our experimental data. In  $\text{MnBi}_2\text{Te}_4$ , the overall anisotropy has contributions from interlayer exchange anisotropy [23], but this contribution will be reduced in  $\text{MnBi}_4\text{Te}_7$  due to the overall weaker exchange coupling.

Magnetization and transport data  $\text{MnBi}_4\text{Te}_7$  are consistent with weaker interlayer AF coupling and dominant uniaxial magnetic anisotropy. Within the Stoner-Wohlfarth model, this weakening results in low-field spin-flip transitions with extremely low coercivity. This is borne out by magnetization and Hall measurements [9] where metamagnetism is heavily dominated by uniaxial anisotropy.

Finally, our results suggest that the intralayer interactions are transferable across the whole MBT family and play a decisive role in the magnetization dynamics of a single-layer magnet where  $n$  is large. The FM nearest-neighbor interaction  $J_1$  is the dominant interaction, and a competing AFM  $J_2$  somewhat destabilizes the FM Mn planes. Both systems also display a relatively long-range neighbor  $J_5$  with comparable strength to  $J_2$ .  $J_5$  is in the

TABLE I. Comparison of the strength of intralayer magnetic coupling  $SJ_{ij}$  (meV) in  $\text{MnBi}_4\text{Te}_7$  and  $\text{MnBi}_2\text{Te}_4$ 

	$SJ_1$	$SJ_2$	$SJ_3$	$SJ_4$	$SJ_5$	$SJ_6$	$SJ_7$	$SJ_8$	$SJ_9$
$\text{MnBi}_4\text{Te}_7$	-0.220(2)	0.035(2)	-0.012(2)	0.009(2)	-0.029(1)	0.014(2)	-0.007(1)	-0.009(1)	-0.009(1)
$\text{MnBi}_2\text{Te}_4$	-0.233(2)	0.033(2)	-0.007(2)	0.003(1)	-0.016(2)	-0.013(2)	-0.008(1)	–	–

same crystallographic  $a$ -axis direction as  $J_1$  at distance of  $3a$  and provides third order harmonics to  $J(q)$  that lead to the distinct linear dispersion relation along  $(H, 0, 0)$ .

## V. CONCLUSIONS

We have measured the spin wave dispersion of the antiferromagnetic topological insulator  $\text{MnBi}_4\text{Te}_7$ . The interactions are strongly two-dimensional in character. However, the key magnetic energy scales within a single septuple block, the single-ion anisotropy and the intralayer exchanges, are transferable to all members of the MBT family.

## ACKNOWLEDGMENTS

This work is supported by the U.S. Department of Energy, Office of Basic Energy Sciences, Division of Materials Sciences and Engineering. Ames Laboratory is operated for the U.S. Department of Energy by Iowa State University under Contract No. DE-AC02-07CH11358. This research used resources at the Spallation Neutron Source, a DOE Office of Science User Facility operated by the Oak Ridge National Laboratory.

## VI. DATA AVAILABILITY

The data that support the findings of this article are openly available [30].

- 
- [1] M. M. Otrokov, T. V. Menshchikova, M. G. Vergniory, I. P. Rusinov, A. Yu Vyazovskaya, Y. M. Koroteev, G. Bihlmayer, A. Ernst, P. M. Echenique, A. Arnau, et al., Highly-Ordered Wide Bandgap Materials for Quantized Anomalous Hall and Magnetoelectric Effects, *2D Mater.* **4**, 025082 (2017).
- [2] M. M. Otrokov, I. I. Klimovskikh, H. Bentmann, D. Estyunin, A. Zeugner, Z. S. Aliev, S. Gaß, A. U. B. Wolter, A. V. Koroleva, A. M. Shikin, et al., Prediction and Observation of an Antiferromagnetic Topological Insulator, *Nature* **576**, 416 (2019).
- [3] J.-Q. Yan, Q. Zhang, T. Heitmann, Z. Huang, K. Y. Chen, J. G. Cheng, W. Wu, D. Vaknin, B. C. Sales, and R. J. McQueeney, Crystal growth and magnetic structure of  $\text{MnBi}_2\text{Te}_4$ , *Phys. Rev. Mater.* **3**, 064202 (2019).
- [4] D. Zhang, M. Shi, T. Zhu, D. Xing, H. Zhang, and J. Wang, Topological Axion States in the Magnetic Insulator  $\text{MnBi}_2\text{Te}_4$  with the Quantized Magnetoelectric Effect, *Phys. Rev. Lett.* **122**, 206401 (2019).
- [5] Y. Deng, Y. Yu, M. Z. Shi, Z. Guo, Z. Xu, J. Wang, X. H. Chen, and Y. Zhang, Quantum anomalous Hall effect in intrinsic magnetic topological insulator  $\text{MnBi}_2\text{Te}_4$ , *Science* **367**, 895 (2020).
- [6] C. Liu, Y. Wang, H. Li, Y. Wu, Y. Li, J. Li, K. He, Y. Xu, J. Zhang, and Y. Wang, Robust axion insulator and Chern insulator phases in a two-dimensional antiferromagnetic topological insulator, *Nat. Mater.* **19**, 522 (2020).
- [7] A. Gao, Y.-F. Liu, C. Hu, J.-X. Qiu, C. Tzschaschel, B. Ghosh, S.-C. Ho, D. Bérubé, R. Chen, H. Sun et al. (2021). Layer Hall effect in a 2D topological axion antiferromagnet. *Nature* **595**, 521 (2021).
- [8] S.K. Chong, Y. Cheng, H. Man, et al., Intrinsic exchange biased anomalous Hall effect in an uncompensated antiferromagnet  $\text{MnBi}_2\text{Te}_4$ , *Nature Communications* **15**, 2881 (2024).
- [9] A. Tan, V. Labracherie, N. Kunchur, A. U. B. Wolter, J. Cornejo, J. Dufouleur, B. Büchner, A. Isaeva, and R. Giraud, Metamagnetism of Weakly Coupled Antiferromagnetic Topological Insulators, *Phys. Rev. Lett.* **124**, 197201 (2020).
- [10] R. C. Vidal, A. Zeugner, J. I. Facio, R. Ray, M. H. Haghighi, A. U. B. Wolter, L. T. Corredor Bohorquez, F. Cagliaris, S. Moser, T. Figgemeier et al., Topological Electronic Structure and Intrinsic Magnetization in  $\text{MnBi}_4\text{Te}_7$ : A  $\text{Bi}_2\text{Te}_3$  Derivative with a Periodic Mn Sublattice, *Phys. Rev. X* **9**, 041065 (2019).
- [11] J. Wu, F. Liu, M. Sasase, K. Ienaga, Y. Obata, R. Yukawa, K. Horiba, H. Kumigashira, S. Okuma, T. Inoshita et al., Natural van der Waals heterostructural single crystals with both magnetic and topological properties, *Sci. Adv.* **5**, eaax9989 (2019).
- [12] J.-Q. Yan, Y. H. Liu, D. S. Parker, Y. Wu, A. A. Aczel, M. Matsuda, M. A. McGuire, and B. C. Sales, A-type antiferromagnetic order in  $\text{MnBi}_4\text{Te}_7$  and  $\text{MnBi}_6\text{Te}_{10}$  single crystals, *Phys. Rev. Mater.* **4**, 054202 (2020).
- [13] L. Ding, C. Hu, F. Ye, E. Feng, N. Ni, and H. Cao, Crystal and magnetic structures of magnetic topological insulators  $\text{MnBi}_2\text{Te}_4$  and  $\text{MnBi}_4\text{Te}_7$ , *Phys. Rev. B* **101**, 020412 (2020).
- [14] I. I. Klimovskikh, M. M. Otrokov, D. Estyunin, S. V. Ereemeev, S. O. Filnov, A. Koroleva, E. Shevchenko, V. Voroshnin, A. G. Rybkin, I. P. Rusinov et al., Tunable 3D/2D magnetism in the  $(\text{MnBi}_2\text{Te}_4)(\text{Bi}_2\text{Te}_3)_m$  topological insulators family, *npj Quantum Mater.* **5**, 54 (2020).
- [15] M. Ceccardi, A. Zeugner, L. C. Folkers, C. Hess, B. Büchner, D. Marré, A. Isaeva, and F. Cagliaris, Anomalous Nernst effect in the topological and magnetic material  $\text{MnBi}_4\text{Te}_7$ , *Npj Quantum Mater.* **8**, 76 (2023).

- [16] J. Wu, F. Liu, C. Liu, Y. Wang, C. Li, Y. Lu, S. Matsuishi, and H. Hosono, Toward 2D Magnets in the  $(\text{MnBi}_2\text{Te}_4)(\text{Bi}_2\text{Te}_3)_n$  Bulk Crystal, *Adv. Mater.* **32**, 2001815 (2020).
- [17] W. Ge, J. Kim, Y.-T. Chan, D. Vanderbilt, J. Yan, and W. Wu, Direct Visualization of Surface Spin-Flip Transition in  $\text{MnBi}_4\text{Te}_7$ , *Phys. Rev. Lett.* **129**, 107204 (2022).
- [18] G. Yu, C. Tang, Z. Tian, Z. Zhu, P. Liu, A. Pan, M. Chen, and X.-Q. Chen, Ferroelectrically Switchable Magnetic Multistates in  $\text{MnBi}_2\text{Te}_4(\text{Bi}_2\text{Te}_3)_n$  and  $\text{MnSb}_2\text{Te}_4(\text{Bi}_2\text{Te}_3)_n$  ( $n = 0,1$ ) Thin Films, *Phys. Rev. B* **108**, 014106 (2023).
- [19] J. Cui, B. Lei, M. Shi, Z. Xiang, T. Wu, and X. Chen, Layer-Dependent Magnetic Structure and Anomalous Hall Effect in the Magnetic Topological Insulator  $\text{MnBi}_4\text{Te}_7$ , *Nano Lett.* **23**, 1652 (2023).
- [20] J. Guo et al., Interlayer coupling modulated tunable magnetic states in superlattice  $\text{MnBi}_2\text{Te}_4(\text{Bi}_2\text{Te}_3)_n$  topological insulators, *Phys. Rev. B* **109**, 165410 (2024).
- [21] C. Hu, L. Ding, K. N. Gordon, B. Ghosh, H.-J. Tien, H. Li, A. G. Linn, S.-W. Lien, C.-Y. Huang, S. Mackey, J. Liu, P. V. S. Reddy, B. Singh, A. Agarwal, A. Bansil, M. Song, D. Li, S.-Y. Xu, H. Lin, H. Cao, T.-R. Chang, D. Dessau, et al., Realization of an Intrinsic Ferromagnetic Topological State in  $\text{MnBi}_8\text{Te}_{13}$ , *Sci. Adv.* **6**, eaba4275 (2020).
- [22] Bing Li, D. M. Pajerowski, S. X. M. Riberolles, Liqin Ke, J.-Q. Yan, and R. J. McQueeney, Quasi-two-dimensional ferromagnetism and anisotropic interlayer couplings in the magnetic topological insulator  $\text{MnBi}_2\text{Te}_4$ , *Phys. Rev. B* **104**, L220402 (2021).
- [23] Bing Li, J.-Q. Yan, D. M. Pajerowski, E. Gordon, A.-M. Nedić, Y. Sizyuk, L. Ke, P. P. Orth, D. Vaknin, and R. J. McQueeney, Competing Magnetic Interactions in the Antiferromagnetic Topological Insulator  $\text{MnBi}_2\text{Te}_4$ , *Phys. Rev. Lett.* **124**, 167204 (2020).
- [24] You Lai, Liqin Ke, Jiaqiang Yan, Ross D. McDonald, and Robert J. McQueeney, Defect-Driven Ferrimagnetism and Hidden Magnetization in  $\text{MnBi}_2\text{Te}_4$ , *Phys. Rev. B* **103**, 184429 (2021).
- [25] C. Lei, O. Heinonen, A. H. MacDonald, and R. J. McQueeney, Metamagnetism of Few-Layer Topological Antiferromagnets, *Phys. Rev. Mater.* **5**, 064201 (2021).
- [26] S. Yang, X. Xu, Y. Zhu, R. Niu, C. Xu, Y. Peng, X. Cheng, X. Jia, Y. Huang, X. Xu et al., Odd-Even Layer-Number Effect and Layer-Dependent Magnetic Phase Diagrams in  $\text{MnBi}_2\text{Te}_4$ , *Phys. Rev. X* **11**, 011003 (2021).
- [27] C. Lei, T. V. Trevisan, O. Heinonen, R. J. McQueeney, and A. H. MacDonald, Quantum anomalous Hall effect in perfectly compensated collinear antiferromagnetic thin films, *Phys. Rev. B* **106**, 195433 (2022).
- [28] See Supplemental Material at <https://journals.aps.org/prb/supplemental/10.1103/PhysRevB.111.064418> for detailed description of background subtraction and model fitting. Further details about the estimation of the transition temperature  $T_N$  and dipolar interaction can also be found there (see Ref. [29]).
- [29] D. Dahlbom, C. Miles, H. Zhang, C. D. Batista, and K. Barros, Langevin dynamics of generalized spins as  $\text{SU}(N)$  coherent states, *Phys. Rev. B* **106**, 235154 (2022).
- [30] Bing Li, R. J. McQueeney, and D. M. Pajerowski, Spin dynamics in the antiferromagnetic topological insulator  $\text{MnBi}_4\text{Te}_7$ , <https://doi.org/10.14461/oncat.data/2499463>.